Article

Quantifying the Congruence between Air and Land Surface Temperatures for Various Climatic and Elevation Zones of Western Himalaya

Shaktiman Singh [1],*, **Anshuman Bhardwaj** [1], **Atar Singh** [2], **Lydia Sam** [1], **Mayank Shekhar** [3], **F. Javier Martín-Torres** [1,4] **and María-Paz Zorzano** [1,5]

[1] Division of Space Technology, Department of Computer Science, Electrical and Space Engineering, Luleå University of Technology, 97187 Luleå, Sweden; anshuman.bhardwaj@ltu.se (A.B.); lydia.sam@ltu.se (L.S.); javier.martin-torres@ltu.se (F.J.M.-T.); zorzanomm@cab.inta-csic.es (M.-P.Z.)

[2] Department of Environmental Science, Sharda University, Greater Noida 201310, India; 2015002854atar@dr.sharda.ac.in

[3] Birbal Sahni Institute of Palaeosciences, Lucknow 226007, India; mayank_shekhar@bsip.res.in

[4] Instituto Andaluz de Ciencias de la Tierra (CSIC-UGR), Armilla, 18100 Granada, Spain

[5] Centro de Astrobiología (INTA-CSIC), Torrejón de Ardoz, 28850 Madrid, Spain

* Correspondence: shaktiman.singh@ltu.se; Tel.: +46-920-492-043

check for updates

Abstract: The surface and near-surface air temperature observations are primary data for glacio-hydro-climatological studies. The in situ air temperature (T_a) observations require intense logistic and financial investments, making it sparse and fragmented particularly in remote and extreme environments. The temperatures in Himalaya are controlled by a complex system driven by topography, seasons, and cryosphere which further makes it difficult to record or predict its spatial heterogeneity. In this regard, finding a way to fill the observational spatiotemporal gaps in data becomes more crucial. Here, we show the comparison of T_a recorded at 11 high altitude stations in Western Himalaya with their respective land surface temperatures (T_s) recorded by Moderate Resolution Imagining Spectroradiometer (MODIS) Aqua and Terra satellites in cloud-free conditions. We found remarkable seasonal and spatial trends in the T_a vs. T_s relationship: (i) T_s are strongly correlated with T_a (R^2 = 0.77, root mean square difference (RMSD) = 5.9 °C, n = 11,101 at daily scale and R^2 = 0.80, RMSD = 5.7 °C, n = 3552 at 8-day scale); (ii) in general, the RMSD is lower for the winter months in comparison to summer months for all the stations, (iii) the RMSD is directly proportional to the elevations; (iv) the RMSD is inversely proportional to the annual precipitation. Our results demonstrate the statistically strong and previously unreported T_a vs. T_s relationship and spatial and seasonal variations in its intensity at daily resolution for the Western Himalaya. We anticipate that our results will provide the scientists in Himalaya or similar data-deficient extreme environments with an option to use freely available remotely observed T_s products in their models to fill-up the spatiotemporal data gaps related to in situ monitoring at daily resolution. Substituting T_a by T_s as input in various geophysical models can even improve the model accuracy as using spatially continuous satellite derived T_s in place of discrete in situ T_a extrapolated to different elevations using a constant lapse rate can provide more realistic estimates.

Keywords: Himalaya; land surface temperature; air temperature; topography; MODIS

1. Introduction

Air temperature (T_a) is an important proxy for energy exchange between land-surface and atmosphere, making T_a one of the most important parameters in climate research [1,2]. T_a is generally

observed at a height of about 2 m above the land surface and it is considered as a critical parameter for glacio-hydrological studies because it controls the rate of melting of snow and ice and the proportion of form of precipitation [3,4]. In addition, it also regulates the evolution of flora and fauna in an area, ultimately controlling the evolution of the ecological niche [5]. T_a is also important for determining the atmospheric water vapor saturation point and thus for the formation of fogs and clouds. The gradient between the air and ground temperature is relevant for estimating the sensible heat flux (i.e., the convective heat flux loss from surface to the air) for calculations of the surface energy balance [6]. The surface-to-air temperature difference is particularly important for evapotranspiration [7]. In other regions, such as the Arctic, the T_a difference is taken as a critical parameter to monitor climate change [8]. Therefore, it is imperative to have accurate estimates of T_a for various natural science disciplines including glaciology, hydrology, ecology, and climatology. The measurement of T_a using in situ automatic meteorological stations is cost intensive due to involved instrumentation and maintenance which makes the spatial continuity of data sparse, particularly in remote environments. This spatially discontinuous nature of in situ T_a measurements adds uncertainty in geospatial modelling in mountainous terrain when the T_a representing single data points are extrapolated to a continuous surface based on fixed lapse rates [9–11].

The land surface temperature (T_s) in a remote sensing perspective is the measure of how hot or cold the top canopy skin layer of the Earth at a particular location will feel when touched [12]. The measure of T_s is largely dependent on net solar radiation, sensible heat flux, reflectance property of the surface, aerodynamic resistance, and the density of air [13]. Although the T_s is closely related to T_a, it can be significantly influenced by the surface characteristics, buffering effects of vegetation and the periodicity of the shortwave radiation emitted from the sun [14]. Over the past decade, the remotely-sensed T_s measurements have been used to map permafrost in different parts of the world [14–17]. There have been several attempts to estimate T_a using remotely-sensed T_s in different ecological systems [18–22]. The root mean square difference (RMSD) between T_a from meteorological stations and T_s from Moderate Resolution Imagining Spectroradiometer (MODIS) on Terra [23] and Aqua [24] satellites was estimated to be ±2.20 °C in Indo-Gangetic plain [25], ±1.33 °C in Portugal [18], ±5.48 °C in mountainous regions of Nevada, United states of America [19], ±2.97 to ±7.45 °C in northern Tibetan Plateau, China [26], ±4.09 to ±4.53 °C in a mountainous region of sub-Arctic Canada [27], and ±1.51 to ±3.74 °C over different ecosystems in Africa [22]. A recent study attempted to analyze the temperature trend using the 8-day T_s corrected using the difference between T_s and T_a calculated for 87 meteorological stations in the Chinese part of Himalaya and Tibetan Plateau [28]. Most of these published studies have compared the T_a and T_s at monthly or 8-day scales while several prominently used ecological and glacio-hydrological models in Himalaya that require daily temperature data as input parameter [4,29]. Moreover, such comparative studies for high mountains of Central or Western parts of Himalaya are completely missing.

The observed temperatures in Himalaya are scarce and fragmented in spatiotemporal domain due to difficult terrain, inhospitable weather conditions, and logistic difficulties in setting-up the weather stations [29]. The Himalayan mountains serve as a source of fresh water supply [30,31] and hydropower generation [32] to the densely populated mountainous regions of Indian Subcontinent. The Himalayan rivers mainly consist of the meltwaters coming from snow and glaciers [30] and this runoff is largely dependent on the seasonal temperatures [4,33]. The glaciers in Himalaya are losing mass in general with a few exceptions [29,33]. However, the quantification of the changes evident in glacierized regions in Himalaya with respect to the changing temperatures are largely uncertain due to unavailability of well-distributed and spatiotemporally continuous network of meteorological stations [29]. Furthermore, the lack of a definite and abiding framework for mutual climatological data sharing among various research and academic organizations in Himalayan countries makes regional-scale glacio-hydro-climatological modelling and interpretations more uncertain [29]. In this respect, there are two significant research gaps: (i) the studies comparing T_a with T_s for a large spatial domain are completely missing for the Central and Western Himalaya, and (ii) owing to this research

gap, the glacio-hydrological community is further unsure of the significant role that spatiotemporally continuous satellite-derived surface temperatures can play as a substitute for spatially discontinuous T_a observations. The land-surface temperature is more likely proxy of energy exchange between land-surface and atmosphere for phenomena which are more strongly linked to ground processes [27]. The main aim of the present study is to understand and quantify the statistically significant trends in $T_s - T_a$ variation over a large spatiotemporal domain in Western Himalaya. Here, we start with providing a description of the study area, followed by data and used methods, and finally we discuss and conclude the main findings of the analyses.

2. Study Area

In the present paper, we analyze the relationship between daily and 8-day mean T_a from 11 high-altitude weather stations (Table 1) in Western Himalaya (Figure 1) and the respective daily and 8-day mean T_s measured by MODIS. The daily and 8-day night- and day-time T_s observations from Version 6 of Terra MODIS (MOD11A1 and MOD11A2 available from February, 2000) and Aqua MODIS (MYD11A1 and MYD11A2 available from July, 2002) were used to calculate average daily and 8-day T_s, respectively.
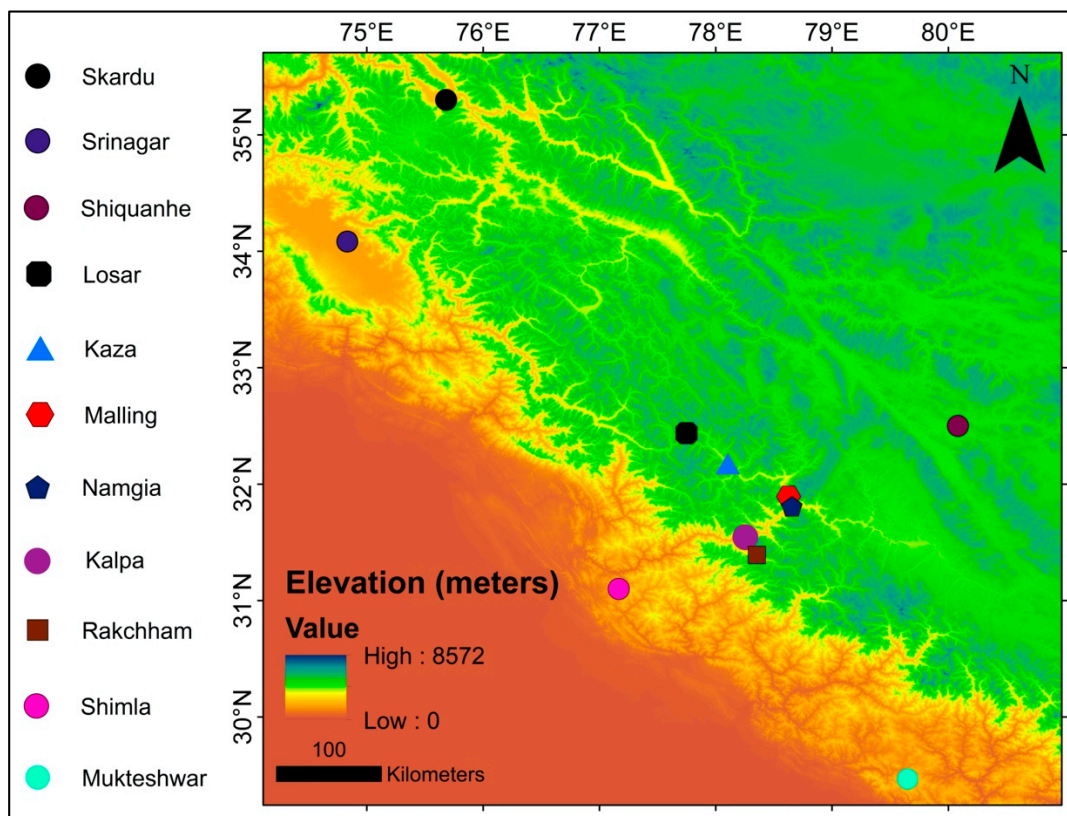

Figure 1. The map showing the location of the stations considered in the study for comparison of land surface temperature (T_s) and air temperature (T_a) with elevation (Aster GDEM v2, 2011) profile of the region.

The stations in the present study are located over a large elevation range above sea level (1587–4280 m) (Figure 1). All the stations used in the analysis are located above 2100 m except for Srinagar which is located at 1587 m. These stations are located in three different Himalayan states of India namely Uttarakhand, Himachal Pradesh, and Jammu and Kashmir. In addition, we have also included one station (Shiquanhe) from the Chinese part of the region in the study (Figure 1). These stations represent various precipitation regimes of the region such as monsoon dominance, westerly

dominance, the precipitation-transition zone from monsoon-to-westerly dominance, and orographic precipitation-shadow zone. The topographic variations, i.e., altitudes and orography, among the Himalayan ranges not only govern the temperatures but also the precipitation [34]. Here, we aim to further untangle the degree of control of the altitude and orography in deciding the correlation between T_s and T_a in the Himalaya.

Table 1. Details of meteorological stations used for comparison in the present study.

Sl. No.	Name of the Station	Elevation (m)	Period	Organization	Precipitation Regime
1.	Kalpa	2707	07-Jul-02–31-Dec-09	IMD	Transition
2.	Kaza	3631	07-Jul-02–31-Dec-09	IMD	Shadow
3.	Namgia	2832	07-Jul-02–31-Dec-09	BBMB	Transition
4.	Rakchham	3046	07-Jul-02–31-Dec-09	BBMB	Transition
5.	Malling	3588	07-Jul-02–31-Dec-09	BBMB	Transition
6.	Losar	4122	07-Jul-02–31-Dec-09	BBMB	Shadow
7.	Mukteshwar	2311	13-Dec-15–30-Sept-19	GHCN	Monsoon
8.	Shimla	2202	01-Jan-16–30-Sept-19	GHCN	Monsoon
9.	Shiquanhe	4280	06-Jul-02–30-Sept-19	GHCN	Shadow
10.	Skardu	2181	02-Oct-02–30-Sept-19	GHCN	Shadow
11.	Srinagar	1587	05-Jul-02–30-Sept-19	GHCN	Shadow

3. Materials and Methods

3.1. Air Temperature (T_a)

The T_a is generally observed at a height of about 2 m above the land surface. T_a data observed at 11 different stations was used in the present study (Table 1). The data for five stations from Global Historical Climatology Network (GHCN) which was acquired from National Centre for Environmental Information (NCEI), NOAA web portal (https://www.ncei.noaa.gov/) [35] had observed daily mean T_a estimated using hourly or 6-hourly observations (Version 3). For the other six stations of Bhakra Beas Management Board (BBMB) and India Meteorology Department (IMD), the T_a was calculated using the daily maximum and minimum observations due to unavailability of daily mean T_a. This method of averaging the daily maximum and minimum temperatures for calculation daily mean temperature is widely used due to the instrumentation, logistic, and computational simplicity [36]. Although the method produces bias in the output due to inability to track the diurnal asymmetry [37], it has been used by considerable number of studies to make acceptable estimates requiring T_a [36]. In order to understand the degree of bias for our study area, we compared the given daily mean T_a with mean of daily maximum and minimum T_a for the five stations of GHCN for which all the three parameters were available. The analysis showed that the RMSD was less than 1.62 °C with a very high correlation ($R^2 > 0.96$) for all the stations. In addition to the daily T_a, we also calculated 8-day mean T_a for comparison with the corresponding 8-day T_s explained in next section. The observations were carefully checked for systematic and random errors before using it for further comparison. The stations used in the present study are distributed broadly over four different precipitation zones (Table 1, Figure 1). The precipitation varies significantly in these precipitation zones. The monsoon dominated, transition zone, westerlies dominated, and precipitation shadow zone receive >1500, 200–800, 600–800, and <150 mm total annual precipitation on an average, respectively.

3.2. MODIS Data

The daily, and 8-day night- and day-time T_s from MODIS satellites on Terra (MOD11A1 and MOD11A2 available from February, 2000) and Aqua (MYD11A1 and MYD11A2 available from July, 2002) satellites [23,24] was downloaded from NASA Earthdata portal (https://earthdata.nasa.gov/) [38] and was used to calculate average of daily and 8-day T_s (Table 2). The remotely-sensed T_s from

MODIS (version 006) has been observed to have RMSD of less than 0.5 K in comparison to the in situ measurements of the T_s [39] and therefore has been widely used for multiple scientific applications [18,19,22,25–28,40].

Table 2. Details of Moderate Resolution Imagining Spectroradiometer (MODIS) data used in the present study.

Sl. No.	Data Characteristics	Terra		Aqua	
		MOD11A1	MOD11A2	MYD11A1	MYD11A2
1.	Temporal resolution	Daily	8-day	Daily	8-day
2.	Spatial resolution	1 km		1 km	
3.	Available from	February, 2000		July, 2002	
4.	Local day time of observation	10:30–11:30		12:30–13:30	
5.	Local night time of observation	21:30–22:30		00:30–01:30	

The local time for the pass over the study area for Terra is around 10:30 and 22:30 and for Aqua is around 13:30 and 01:30 during day and night, respectively. The 8-day land surface temperature data MOD11A2 and MYD11A2 is a simple pixel wise average of all the respective MOD11A1 and MYD11A2 data collected during the 8-day period. The days with all the four observations, including the day and night-time measurements available from both Terra and Aqua were included in the comparison at both daily and 8-day scale. Equation (1) was used to compute the average of four MODIS observations during a day or 32 MODIS observations during an 8-day period (referred as T_s in °C) from the pixel value corresponding to every station given in Table 1.

$$T_s = \frac{T_d^T + T_n^T + T_d^A + T_n^A}{4} - c,$$ (1)

where,

T_d^T = Terra day-time observation
T_n^T = Terra night-time observation
T_d^A = Aqua day-time observation
T_n^A = Aqua night-time observation
c = Constant for conversion from kelvin to Celsius (273.15)

For every data point of daily and 8-day T_s, two night-time and two day-time satellite observations were used. It moderated the calculated daily T_s for further comparison with T_a. Therefore, every data point of daily T_s is average of four MODIS observations during that day and 8-day T_s is average of 32 MODIS observations during that 8-day period. Since, the satellite observation from MODIS is unavailable in cloud cover condition and the calculated daily T_s for comparison with T_a can have large data gaps, we decided to also include MODIS 8-day T_s in the analyses. For 8-day T_s, the data available is comparatively more continuous due to correction of cloud contamination [39]. Although, the 8-day MODIS observations are more efficient in terms of temporal continuity, it compromises with the temporal resolution. Additionally, the number of data points available for comparison for 8-day average is significantly less than the dataset available for daily average. Thus, the average T_s used in our analyses, and referred to hereafter, is essentially the average of four-times daily and 8-day MODIS T_s observations and all the results should be considered accordingly. Therefore, based on these data limitations, we finally compared the average of four-times daily and 8-day MODIS T_s observations with observed daily mean T_a for five GHCN stations and with the average of observed daily maximum and minimum temperatures for the remaining six stations.

3.3. Statistical Analyses

We applied different statistical tools and tests to analyze the relationship between T_s and T_a. Firstly, the coefficient of correlation (r), coefficient of determination (R^2), standard error of regression (SE), and root mean square difference (RMSD) between T_s and T_a for all the stations was calculated. The SE is the standard deviation of the difference between two datasets while RMSD is the square root of mean of squared difference between two datasets. The R^2 explains the efficiency of the regression model. In other words, it is the degree to which the independent variable will be able to explain the dependent variable. During the analysis, the T_a was considered to be the dependent variable (y) and T_s was considered as the independent variable (x). The p-values for all the analyses were <0.01 at 99% confidence level. Additionally, we estimated these statistical parameters for all available data for different climate zones namely monsoon-dominated, transition, westerlies-dominated, and precipitation shadow and for all the stations. The value of modified R^2 which is adjusted for the number of predictors was observed to be around unadjusted R^2 and therefore was not shown in the table. The p-value for each of the analyses was found to be less than 0.01 at 99% confidence level showing the effect of predictors. In addition, we analyzed the variation in the magnitude of the coefficient of the difference between T_s and T_a observed after the multiple regression taking January as the base month. We also plotted the box and whisker plots for the daily difference between T_s and T_a to graphically represent the overall range of the data, median of the data, and distribution of the data in different quartiles.

4. Results

4.1. T_s vs. T_a Relationship

We performed different statistical analyses to derive several first-hand conclusions regarding the relationship between T_s and T_a in the Himalayan region. The results show a strong relationship between observed daily mean T_a and its respective daily mean T_s in general for all the stations (R^2 = 0.77, RMSD = 5.9 °C, SE = 4.76, n = 11,101, p-value <0.01 at 99% confidence level) with variations corresponding to the altitudinal locations of the stations (Figure 2 and Table 3). The strongest relationship between T_a and T_s at daily scale was observed for Shimla (R^2 = 0.94; RMSD = 1.5 °C, SE = 1.2 °C, n = 304, p-value <0.01 at 99% confidence level) and Mukteshwar stations (R^2 = 0.94; RMSD = 1.6 °C, SE = 1.2 °C, n = 355, p-value <0.01 at 99% confidence level) which are located on the southern slopes in monsoon-dominated precipitation regime. The coefficient of determination is considerable for all the stations (R^2 > 0.69, p-value <0.01 at 99% confidence level) at daily scale.

Table 3. Summary of all the statistical tests used for analysis between T_s and T_a for all the stations, climate regimes and for all observations at daily and 8-day scale. (R^2 = Coefficient of determination; SE = Standard Error of Regression; RMSD = Root mean square difference).

| Name of the Station	Observations		R^2		SE		RMSD		Regression Equation	
	Daily	8-day	Daily	8-day	Daily	8-day	Daily	8-day	Daily	8-day
Srinagar	1771	664	0.96	0.97	1.38	1.23	2.7	2.5	$T_a = 0.96T_s - 1.64$	$T_a = 0.92T_s - 0.72$
Skardu	193	35	0.82	0.93	2.06	1.22	4.3	3.2	$T_a = 0.94T_s - 2.67$	$T_a = 0.82T_s - 0.71$
Shimla	304	55	0.94	0.97	1.22	0.96	1.5	1.4	$T_a = 0.97T_s + 1.43$	$T_a = 0.94T_s + 1.78$
Mukteshwar	355	63	0.94	0.96	1.16	1.05	1.6	1.2	$T_a = 1.03T_s + 0.62$	$T_a = 0.99T_s + 0.76$
Kalpa	866	337	0.87	0.89	1.93	1.95	2.7	2.5	$T_a = 0.80T_s + 0.93$	$T_a = 0.83T_s + 0.98$
Namgia	1141	338	0.92	0.95	1.96	1.78	3.0	2.6	$T_a = 0.75T_s + 2.39$	$T_a = 0.79T_s + 2.14$
Rakhham	820	310	0.79	0.88	2.45	2.09	3.1	2.9	$T_a = 0.77T_s + 2.63$	$T_a = 0.79T_s + 2.71$
Malling	1093	332	0.77	0.85	2.83	2.51	5.2	4.5	$T_a = 0.59T_s + 2.51$	$T_a = 0.64T_s + 2.30$
Kaza	1028	333	0.80	0.83	4.29	4.37	7.4	7.2	$T_a = 0.83T_s - 3.92$	$T_a = 0.86T_s - 4.17$
Losar	1019	308	0.69	0.77	7.12	6.59	8.1	7.8	$T_a = 0.81T_s - 2.16$	$T_a = 0.84T_s - 3.23$
Shiquanhe	2511	777	0.88	0.97	3.19	1.56	8.7	8.9	$T_a = 0.82T_s - 6.43$	$T_a = 0.80T_s - 6.46$
Monsoon-Dominated	659	118	0.94	0.96	1.19	1.02	1.5	1.3	$T_a = 1.00T_s + 1.01$	$T_a = 0.96T_s + 1.31$
Transition	3920	1317	0.82	0.88	2.56	2.31	3.7	3.2	$T_a = 0.69T_s + 2.45$	$T_a = 0.74T_s + 2.27$
Westerlies-Dominated	1964	699	0.95	0.97	1.51	1.24	2.9	2.5	$T_a = 0.95T_s - 1.61$	$T_a = 0.91T_s - 0.69$
Precipitation Shadow	4558	1418	0.77	0.85	4.92	4.22	8.4	8.4	$T_a = 0.80T_s - 4.70$	$T_a = 0.80T_s - 5.06$
Overall Observations	11,101	3552	0.77	0.80	4.76	4.49	5.9	5.7	$T_a = 0.87T_s - 1.83$	$T_a = 0.85T_s - 1.63$
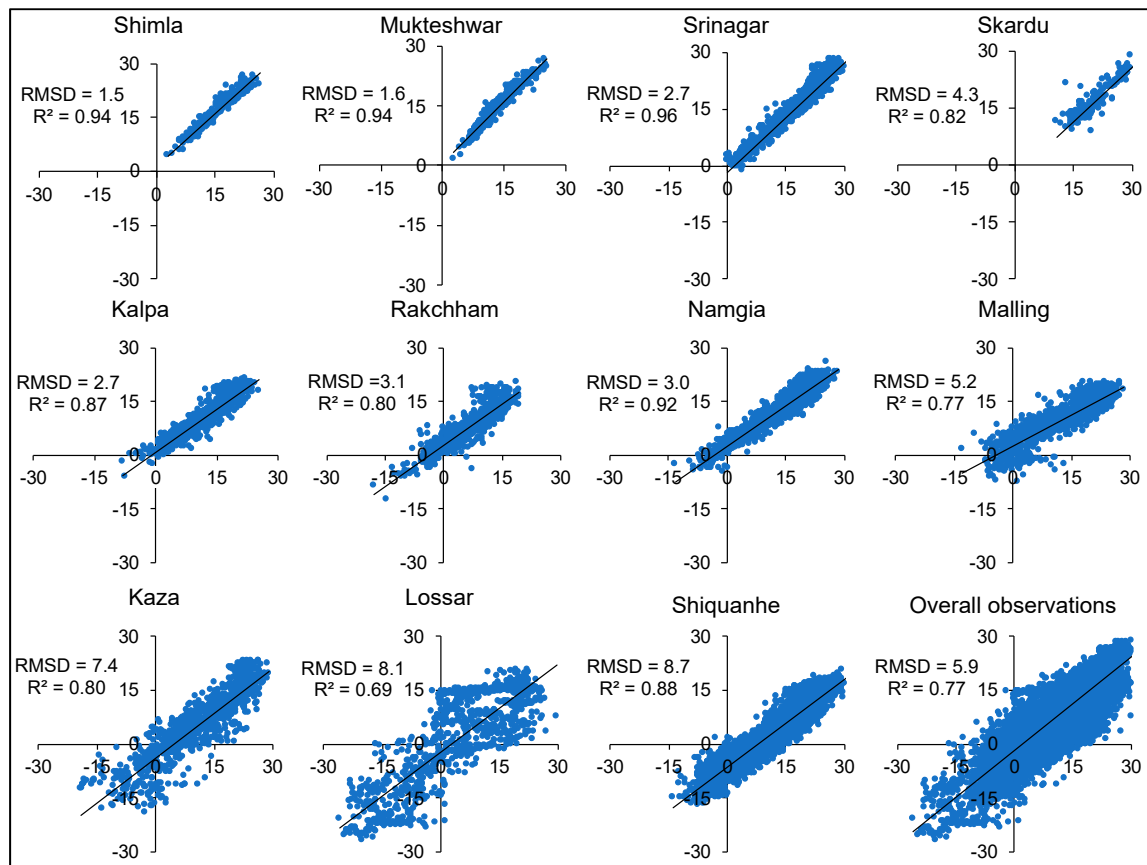
Figure 2. The scatter plot between daily T_s (x-axis) and T_a (y-axis) for all the stations and overall observations with respective coefficient of determination (R^2) and root mean square difference (RMSD) in °C.

The R^2 and RMSD for all the stations show slight improvement for 8-day average (Figure 3 and Table 3). The relationship between T_a and T_s for 8-day average was also found to be strongest for Shimla ($R^2 = 0.97$; RMSD = 1.4 °C, SE = 0.96 °C, $n = 55$, p-value <0.01 at 99% confidence level) and Mukteshwar stations ($R^2 = 0.96$; RMSD = 1.2 °C, SE = 1.05, $n = 63$, p-value <0.01 at 99% confidence level). Overall, the T_a and T_s relationship was found to be stronger ($R^2 = 0.96$; RMSD = 5.7 °C, SE = 4.5, $n = 3552$, p-value <0.01 at 99% confidence level) at 8-day scale for all the stations as well. The regression equation for all the analyses was also given which can be used for estimating T_a for different climate regimes with continuity over large spatiotemporal domain using T_s (Table 3) at both daily and 8-day scales.
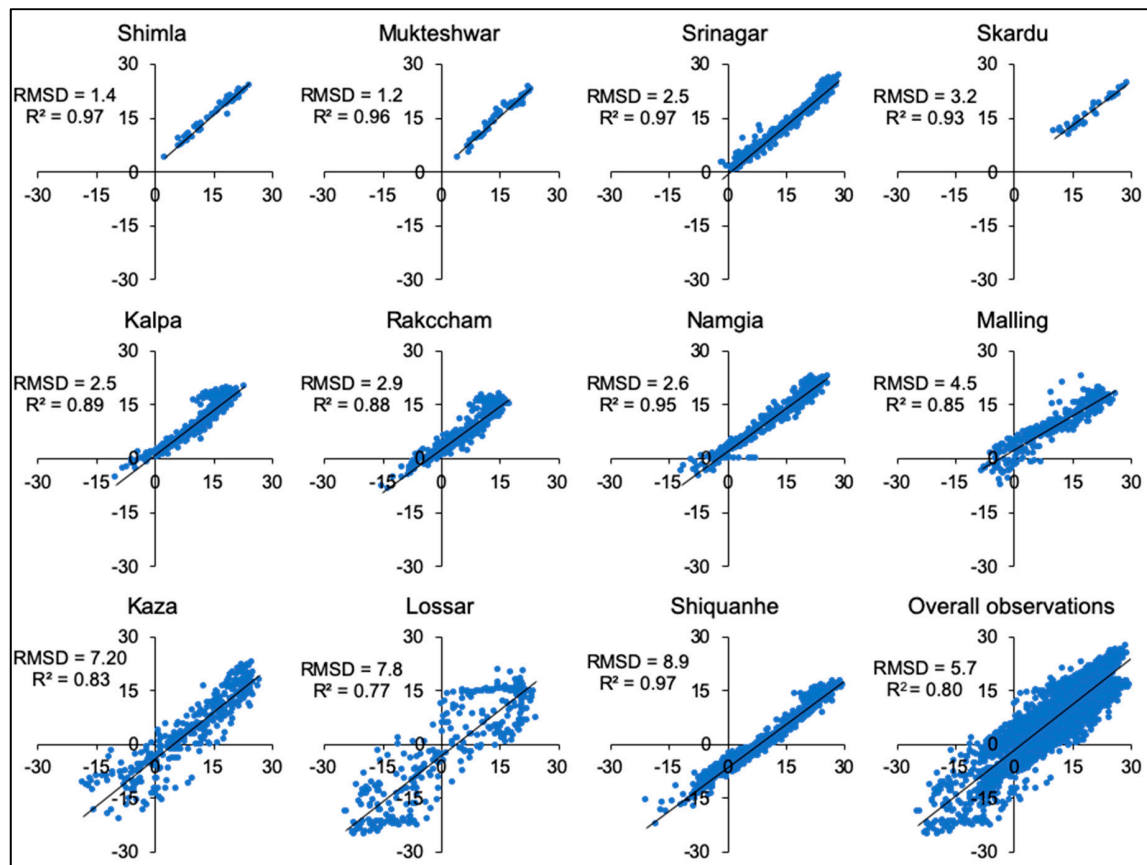
Figure 3. The scatter plot between 8-day T_s (x-axis) and T_a (y-axis) for all the stations and overall observations with respective coefficient of determination (R^2) and RMSD in °C.

The number of data points available for 8-day analysis is significantly less in comparison to the daily analysis (Table 1). Additionally, the use of 8-day data gives spatiotemporal continuity due to correction of cloud contaminated pixels but poses a restriction on the frequency of comparisons. We decided to represent the analysis of the relationship between T_a and T_s at daily scale henceforth because there was very small improvement in the results observed after the use of 8-day data and the daily observation are crucial for different geophysical models as explained in the Introduction section. We noticed certain spatial patterns in the daily differences between T_s and T_a which are discussed in detail in the following paragraphs.

4.2. Altitudinal Relationship

First, we present the relationship between $T_s - T_a$ by considering altitudinal positions of the stations. The variation in altitude affects the T_a due to difference in density of air which causes a reduced green-house effect in the higher reaches. The RMSD between T_s and T_a for stations has a direct correlation with the elevation of the station (Figures 2–4). Although, the RMSD increases systematically with increase in elevation in general, small variation in this trend is observed for northernmost stations (Skardu and Srinagar). The annual mean RMSD is strongly correlated to the elevation ($R^2 = 0.74$) in general (Figure 5a) except for two stations (Skardu and Srinagar), which even when located at comparatively low elevations show higher magnitude of RMSD (Figure 4). The R^2 is stronger for monsoon season (Figure 5b) in comparison to annual (Figure 5a) and summer season values (Figure 5c). The observed T_a was unavailable for Skardu for winter months (Figure 5d). Therefore, the R^2 is highest for winter when compared to monsoon, summer, and annual analysis. Furthermore, the magnitude of $T_s - T_a$ is observed to be higher in summer months in comparison to the winter months for all the stations in general (Figure 4).
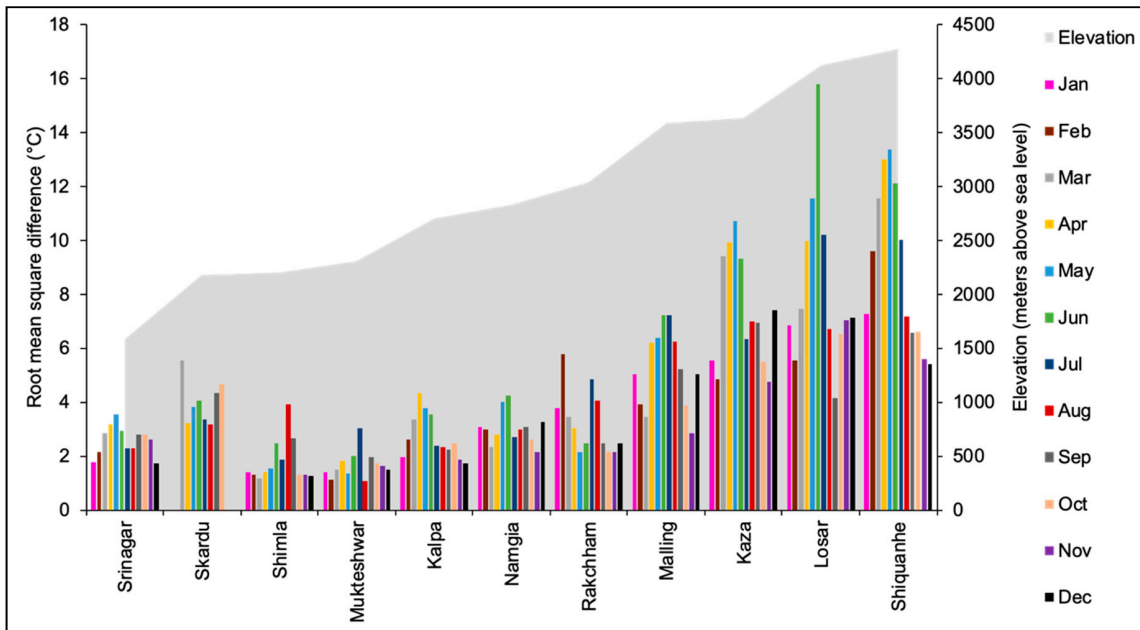
Figure 4. Graph showing the monthly mean of RMSD between daily T_s and T_a for different stations with respective elevation. The RMSD is higher in summer months and increases with increase in elevation.
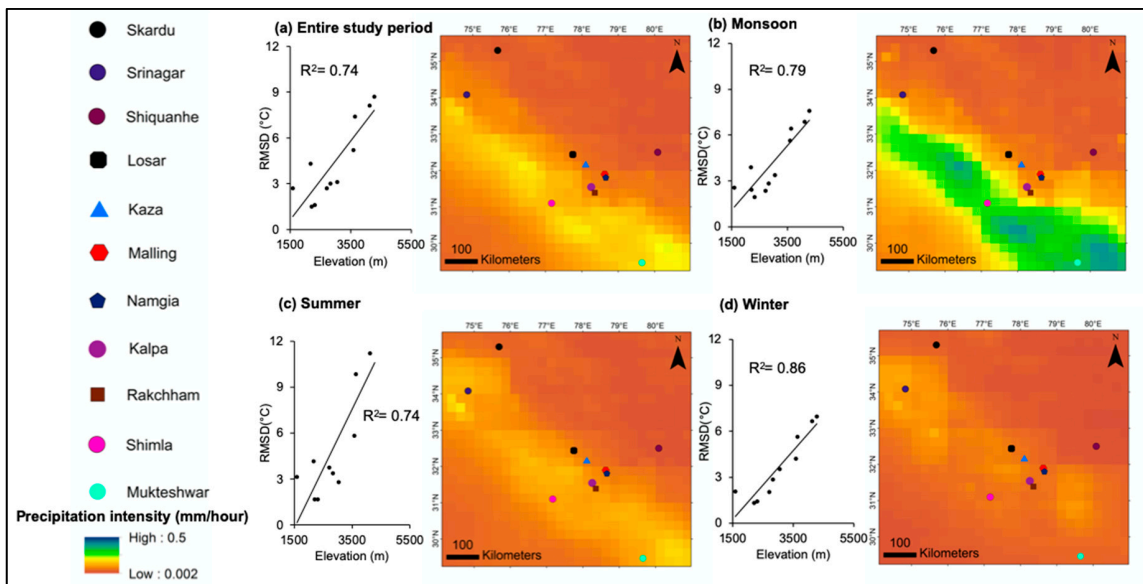

Figure 5. The graph showing the relationship between average of RMSD between daily T_s and T_a for each station and its corresponding elevation for (**a**) the entire study period, (**b**) monsoon (JASO), (**c**) summer (MAMJ), and (**d**) winter (NDJF). The map shows the precipitation intensity (mm/h) data from Tropical Rainfall Measuring Mission (GES DISC, 2016) for the period 1 January 1999 to 31 December 2017 plotted through GIOVAANI (https://giovanni.gsfc.nasa.gov/giovanni/) [41].

4.3. Seasonal Relationship

The difference between mean monthly T_a and T_s (i.e., $T_s - T_a$) for the entire period of study shows high inter-monthly variability for all the stations except for the stations in monsoon-dominated regions (Figures 5 and 6). The mean monthly T_s is lower in comparison to mean monthly T_a for southern slopes (Figure 6a) and increases with increasing latitudes (Figure 6c) except for the stations in westerlies dominated areas (Figure 6d). The magnitude of difference between mean monthly T_s and mean monthly T_a is negative for the stations in monsoon-dominated areas and positive for the stations in precipitation

shadow and westerly-dominated regions. In the precipitation-transition zone, the difference is positive for summer months and negative for winter months except for Rakchham, the southernmost station of the transition zone (Figure 5). For Rakchham, the $T_s - T_a$ values are negative throughout the year similar to the stations in monsoon-dominated areas (Figure 6b). This might be a result of the added effect of humidity in the near-surface atmosphere and presence of snow on land surface which moderates the difference between T_s and T_a [42] throughout the year in monsoon-dominated regions. In the precipitation-transition zone, the difference is partly moderated by the presence of snow during winter months and partly humidity during summer months, particularly for the southernmost stations of the zone (Rakchham and Kalpa) (Figures 5 and 6b) which receive enough precipitation through both monsoon and westerlies. $T_s - T_a$ values for the stations in westerly-dominated region are regulated mainly by the presence of snow during winters (Figures 5 and 6d), which tends to cool the surface due to high albedo [42]. The $T_s - T_a$ values for the stations in precipitation-shadow zone are significantly high and positive in magnitude throughout the year in comparison to all the other stations due to the perennial cold-arid atmospheric conditions (Figures 5 and 6c). This confirms the role of water cycle on this gradient and shows that in the absence of soil-atmosphere water cycle (dry conditions) the magnitude of the difference between $T_s - T_a$ increases and is more positive.
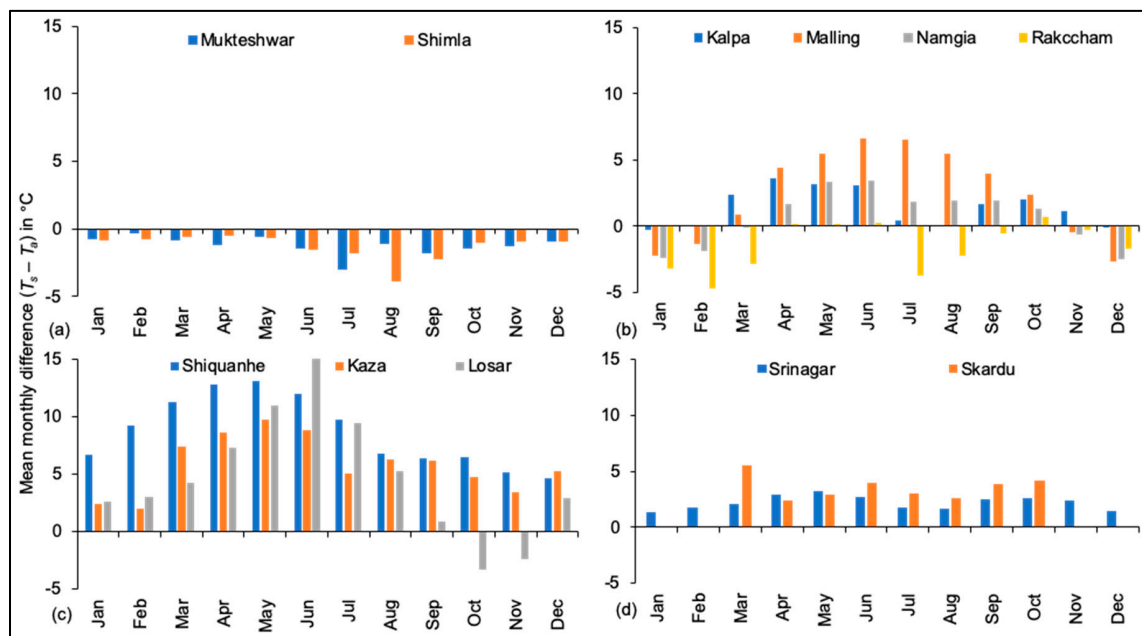

Figure 6. Graph showing the mean monthly difference between daily T_s and T_a for the entire period for which the data is available for stations in (**a**) monsoon-dominated areas, (**b**) transition zone, (**c**) precipitation shadow zone, and (**d**) westerlies-dominated areas. The observed T_a for Skardu for winter months was unavailable. The $T_s - T_a$ values for the stations in the precipitation-shadow zone (**c**) are significantly higher and positive in magnitude, due to the perennial cold-arid atmospheric conditions.

The comparison of T_s and T_a showed high inter-monthly variability throughout the study period. Therefore, we performed an additional analysis where we estimated the seasonal effect of each month on the difference between T_s and T_a (Figure 7) in reference to a base month. For this multiple regression analysis, January was considered as the base month since the $T_s - T_a$ values in January were least for all the stations in general (Figure 6). This analysis further corroborates the above-discussed aspect that the $T_s - T_a$ coefficient values are larger in summer months in comparison to winter months (Figure 7). Additionally, the difference in coefficient and RMSD is high for stations in precipitation shadow regions (Kaza, Shiquanhe and Losar) in comparison to the stations in monsoon-dominated areas (Shimla and Mukteshwar) (Figures 6 and 7).
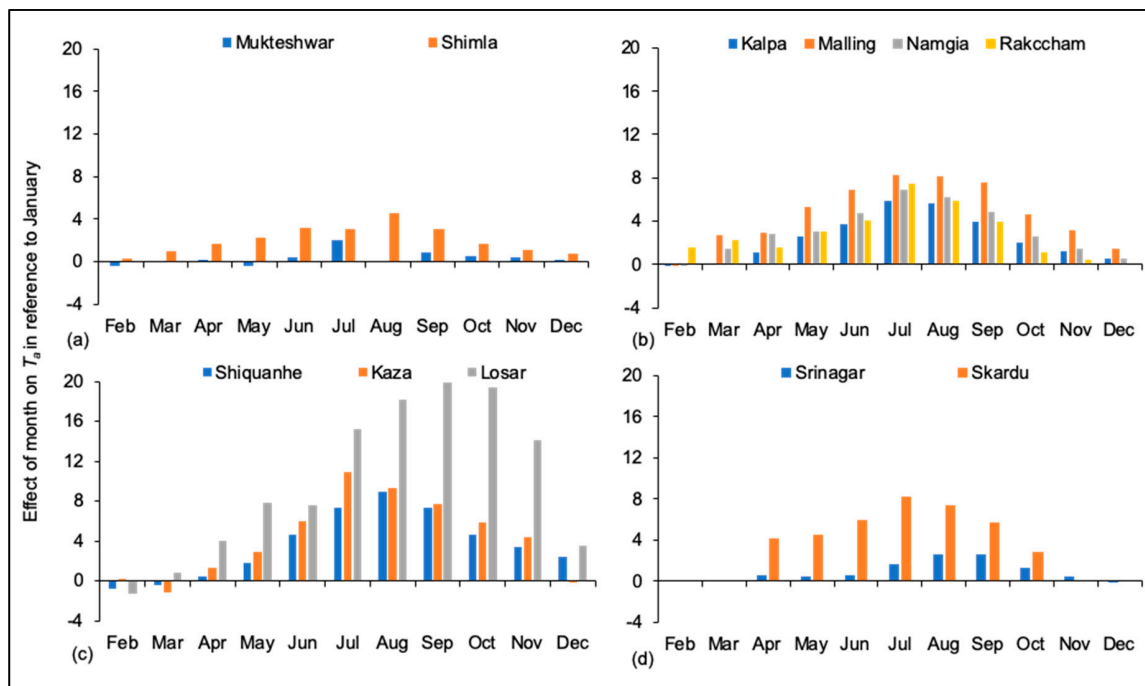
Figure 7. Graph showing the effect of each month on the T_a in reference to the month of January for stations in (**a**) monsoon-dominated areas, (**b**) transition zone, (**c**) precipitation shadow zone, and (**d**) westerlies-dominated areas. The observed T_a for Skardu for winter months was unavailable.

To further corroborate the effect of seasonality and the presence of snow and humidity on the $T_s - T_a$ values, we created monthly box and whisker plots of daily difference between T_s and T_a (Figure 8). The whisker for the stations in precipitation shadow zone and transition zone is longer showing the high monthly variability of the difference value in comparison to the stations in monsoon and westerlies-dominated areas. This is due to the presence of snow during the winter and humidity in the atmosphere in summer regulating the difference between T_s and T_a in the monsoon dominated areas. Additionally, the size of the boxes are smaller for the stations in monsoon and westerlies-dominated areas explaining the presence of maximum data points close to the median representing that throughout the year the difference between T_s and T_a is regulated by presence of snow or atmospheric moisture. On the contrary, the boxes for stations in precipitation shadow zones which receive significantly less precipitation throughout the year, are wider in size representing large variation in the difference between T_s and T_a throughout the year. The boxes for the stations in the southern part of the transition zone are smaller in summer and wider in winter showing the effect of humidity due to some influence of monsoon owing to their spatial closeness to the monsoon-dominated region. Besides, both the boxes and whiskers for the stations in north-eastern part of the transition zone, closer to the precipitation shadow zone, are wider in size showing the variability due to lack of both snow and humidity.
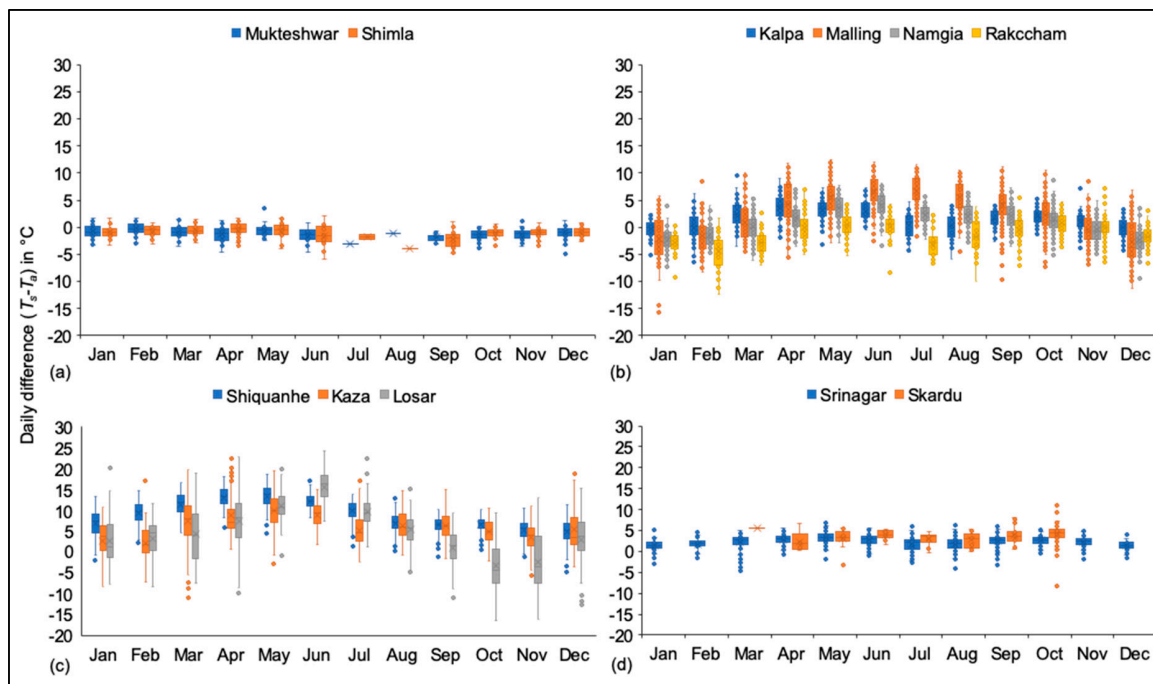
Figure 8. Box and whisker plots showing the monthly variation of daily difference between T_s and T_a for the entire period for which the data is available for stations in (**a**) monsoon-dominated areas, (**b**) transition zone, (**c**) precipitation shadow zone, and (**d**) westerlies-dominated areas.

5. Discussion

The observed near-surface air temperature is one of the most important climate parameters used in different kinds of environmental studies particularly in Himalaya where the interaction between high elevation, climate, and cryosphere is highly significant and complex. It is extremely difficult to capture the spatial heterogeneity of the near-surface temperature [43] which is the primary forcing data for different glacio-hydrological models [3,4,44–46]. It is also used as primary data for climate change assessment [47,48], agro-climatic [40], ecological [49,50], and socio-economic [51,52] studies. Our results present a freely available substitute for station recorded T_a with high temporal and spatial resolution. Conclusively, the T_s is highly correlated with T_a throughout the study area at both daily and 8-day scales. The correlation is highest at the stations located at Southern slope (Shimla and Mukteshwar) with significantly low RMSD in comparison to the stations located in the Eastern part (Losar and Shiquanhe). Although, the degree of congruence between T_s and T_a is slightly higher in the 8-day dataset ($R^2 > 0.77$) in comparison to the daily dataset ($R^2 > 0.69$), the number of data points available for comparison is significantly low. The overall RMSD improved by 0.2 °C on an average by using the 8-day dataset. The largest improvement in RMSD was observed for Skardu (1.1 °C) but the number of data points available for correlation was significantly less than other stations. The overall SE improved by 0.38 °C except for Kalpa and Kaza for which it deteriorated by 0.02 and 0.08 °C, respectively. It is interesting to note that for Shiquanhe which is located in precipitation shadow zone and highest altitude among all the stations, shows largest improvement in SE (by 1.63 °C) and reduction in RMSD (0.2 °C).

The difference between T_s and T_a is primarily controlled by elevation, the land surface cover characteristics, and near-surface humidity. At higher altitudes, the thinner atmosphere shows lesser water holding capacity and the atmosphere saturates faster, thus allowing for lesser evaporation/sublimation in a given pressure-temperature scenario [53]. This puts a constraint on the limit of specific humidity in the high elevations and the comparatively lesser number of available water molecules in the near-surface atmosphere cannot trap the same amount of heat as those at lower elevations. This can provide a basis for the observed high values of $T_s - T_a$ at the higher altitudes. The

intercept of the regression between T_s and T_a shows increase for the stations in monsoon, transition, and westerlies-dominated areas. On the contrary, the stations in precipitation shadow zone show a sharp decrease in the intercept of the regression at high elevations (>3600 m). The slope of the regression between T_s and T_a is higher for stations in low elevation and precipitation-dominated areas (0.80–1.03) in comparison to the stations in high elevation and in transition-to-precipitation shadow zones (0.59–0.86). This observation is supported by a study which shows decrease in slope and degree of correlation in high elevation [54]. The high difference between T_s and T_a for the stations in dry atmosphere at high altitude may partially be due to the heat from the Sun and cooling of near-surface atmosphere due to heat exchange from surrounding air and temperature lapse rate [55]. The presence of more humidity moderates the difference between T_s and T_a in precipitation dominant areas. The difference between T_s and T_a is highest with positive magnitude when the land surface is snow-free and the near-surface atmosphere is dry. On the contrary, the T_s and T_a is negative and lower in magnitude when the land surface is covered by snow and/or atmosphere is more saturated with moisture regardless of high altitude. In addition to the elevation and precipitation regime, season was observed to have significant control over the difference between T_s and T_a. The summer months were observed to have a significantly higher effect on T_a in reference to January, in general for all the stations. The inter-monthly variability was observed to be very high for year-round humidity-deficient transition zones and precipitation shadow zones in comparison to the monsoon-dominated and westerlies-dominated regions. It can be interpreted that the energy exchange between the surface and near-surface atmosphere in the precipitation dominant areas is more efficient in comparison to the precipitation deficient areas.

The lower magnitude of RMSD between T_s and T_a represents lower gradient of temperature between the land surface and near-surface air due to the cold bias caused by snow cover which protects the surface from warming because of its high albedo [42]. A possible contributing factor to this seasonal disparity can be the reported perpetually melting seasonal snow in Himalayan mountains [55] under the changing regional climate. The causal mechanism for this relationship deserves a separate detailed investigation. However, a possible cause of such observations can be linked to the fact that the diurnal temperatures even in the mid-winter months often cross the freezing point causing a certain degree of melting to prevail [56]. This can start a cascading event where during the preliminary warming phase, the average snowpack temperature reaches and stays at 0 °C isotherm until the melting typically starts within the snowpack prior to the ripening phase as meltwater is retained within the snowpack [57]. This meltwater may subsequently refreeze owing to the diurnal cycles of temperature and the latent heat released during this process can additionally warm the snow surface and the surrounding air, further minimizing the temperature difference [56]. In addition to the seasonal change in the land cover characteristics, the variation in humidity in the near-surface atmosphere is an important factor controlling the difference between T_s and T_a. It was recently proposed that the amount of moisture content on the land surface has a cooling effect on land surface temperature [40]. Thus, the precipitation regime in which a particular station is located can further provide us several clues regarding the observed variations in $T_s - T_a$ values. These precipitation regimes have been previously characterized [34] and in the following discussion, we take a focused approach towards revisiting the $T_s - T_a$ variations with respect to the respective precipitation scenarios.

All the statistical results and the regression equation between T_s and T_a have specific trends for particular climate setting and elevation which can be used to estimate T_a using T_s (Table 3) for glacio-hydrological and climate change studies in data-deficient Himalaya. For example, the RMSD ranges between 1.2–1.6, 2.6–5., 2.5–4.3, and 7.2–8.9 °C for the stations in monsoon-dominated, transition, westerlies-dominated, and precipitation shadow zones, respectively, for both daily and 8-day products. The slope and intercept of the regression equations between T_s and T_a are also similar for the stations in the same precipitation regime. The paper demonstrates different patterns of variation of $T_s - T_a$ in different climate regimes within the region of study. Due to the inherent limitations of the available data, some of this analysis may be revised in the future by specific dedicated studies, in particular to

asses if the relationships hold on daily scales and with what error bar. Some possible error sources for this analysis may come from the scarcity of the data, and the fact that we compared data from different instrumentation accuracies and cadences. T_a is measured by three different organizations and two calculation methods are used for daily mean air temperature during different observation periods. The correlation of the instantaneous observation of T_a in relation to satellite derived T_s can be investigated by analyzing the diurnal variation of T_a in relation to the time of pass of the satellite [58]. There are different parameters like wind speed and fractional vegetation which have additional effects on the difference between T_s and T_a, which have not been investigated in the present study [54,55] and can be interesting research questions for future investigations in the region.

6. Conclusions

Unavailability of reliable temperature observations with spatial continuity along with the extreme weather conditions and difficult terrain in the remoteness of Himalaya hampers our understanding of the cryosphere-climate coupling in these mountains. Here we attempt to compare remotely sensed T_s with respect to in situ T_a observations over different precipitation and altitudinal zones of the Western Himalaya. Although, there are several studies available from different parts of the globe attempting to estimate T_a using T_s or vice-versa using monthly or 8-day MODIS data, we provide an understanding of the spatiotemporal variability of the T_a vs. T_s relationship at diurnal scales. The results show a strong and statistically significant relationship between T_s and T_a in general with a spatiotemporal consistency, thus projecting satellite-derived T_s as a viable alternative to the in situ T_a for glacio-hydro-climatological studies. We also provide regression equations to facilitate modeling of gridded T_a using corresponding T_s for different regions of Western Himalaya. MODIS in combination with Sea and Land Surface Temperature Radiometer (SLSTR) onboard Sentinel-3 can provide better capability to overcome cloud gaps and ensuring spatiotemporal continuity for T_s future studies in this direction.

References

1. Hansen, J.; Ruedy, R.; Sato, M.; Lo, K. Global surface temperature change. *Rev. Geophys.* **2010**, *48*, RG4004. [CrossRef]
2. Jones, P.D. Hemispheric Surface Air Temperature Variations: A Reanalysis and an Update to 1993. *J. Clim.* **1994**, *7*, 1794–1802. [CrossRef]
3. Hock, R. Temperature index melt modelling in mountain areas. *J. Hydrol.* **2003**, *282*, 104–115. [CrossRef]
4. Kumar, R.; Singh, S.; Kumar, R.; Singh, A.; Bhardwaj, A.; Sam, L.; Randhawa, S.S.; Gupta, A. Development of a glacio-hydrological model for discharge and mass balance reconstruction. *Water Resour. Manag.* **2016**, *30*, 3475–3492. [CrossRef]
5. Hatfield, J.L.; Prueger, J.H. Temperature extremes: Effect on plant growth and development. *Weather Clim. Extrem.* **2015**, *10*, 4–10. [CrossRef]

6.   Stoll, M.J.; Brazel, A.J. Surface-air temperature relationships in the urban environment of Phoenix, Arizona. *Phys. Geogr.* **1992**, *13*, 160–179. [CrossRef]

7.   Seiler, C.; Moene, A.F. Estimating Actual Evapotranspiration from Satellite and Meteorological Data in Central Bolivia. *Earth Interact.* **2011**, *15*, 1–24. [CrossRef]

8.   Screen, J.A.; Simmonds, I. The central role of diminishing sea ice in recent Arctic temperature amplification. *Nature* **2010**, *464*, 1334. [CrossRef]

9.   Ishida, T.; Kawashima, S. Use of cokriging to estimate surface air temperature from elevation. *Theor. Appl. Climatol.* **1993**, *47*, 147–157. [CrossRef]

10. Snehmani; Bhardwaj, A.; Singh, M.K.; Gupta, R.D.; Joshi, P.K.; Ganju, A. Modelling the hypsometric seasonal snow cover using meteorological parameters. *J. Spat. Sci.* **2015**, *60*, 51–64. [CrossRef]

11. Willmott, C.J.; Robeson, S.M. Climatologically aided interpolation (CAI) of terrestrial air temperature. *Int. J. Climatol.* **1995**, *15*, 221–229. [CrossRef]

12. Bense, V.F.; Read, T.; Verhoef, A. Using distributed temperature sensing to monitor field scale dynamics of ground surface temperature and related substrate heat flux. *Agric. For. Meteorol.* **2016**, *220*, 207–215. [CrossRef]

13. Sellers, P.J.; Dickinson, R.E.; Randall, D.A.; Betts, A.K.; Hall, F.G.; Berry, J.A.; Collatz, G.J.; Denning, A.S.; Mooney, H.A.; Nobre, C.A.; et al. Modeling the exchanges of energy, water, and carbon between continents and the atmosphere. *Science* **1997**, *275*, 502–509. [CrossRef] [PubMed]

14. Luo, D.; Jina, H.; Marchenkoa, S.S.; Romanovsky, V.E. Difference between near-surface air, land surface and ground surface temperatures and their influences on the frozen ground on the Qinghai-Tibet Plateau. *Geoderma* **2018**, *312*, 74–85. [CrossRef]

15. Hachem, S.; Allard, M.; Duguay, C. Using the MODIS land surface temperature product for mapping permafrost: An application to northern Québec and Labrador, Canada. *Permafr. Periglac. Process.* **2009**, *20*, 407–416. [CrossRef]

16. Hachem, S.; Duguay, C.R.; Allard, M. Comparison of MODIS-derived land surface temperatures with ground surface and air temperature measurements in continuous permafrost terrain. *Cryosphere* **2012**, *6*, 51–69. [CrossRef]

17. Ran, Y.; Li, X.; Jin, R.; Guo, J. Remote sensing of the mean annual surface temperature and surface frost number for mapping permafrost in China. *Arct. Antarct. Alp. Res.* **2015**, *47*, 255–265. [CrossRef]

18. Benali, A.; Carvalho, A.C.; Nunes, J.P.; Carvalhais, N.; Santos, A. Estimating air surface temperature in Portugal using MODIS LST data. *Remote Sens. Environ.* **2012**, *124*, 108–121. [CrossRef]

19. Mutiibwa, D.; Strachan, S.; Albright, T. Land Surface Temperature and Surface Air Temperature in Complex Terrain. *IEEE J. Sel. Top. Appl. Earth Obs. Remote Sens.* **2015**, *8*, 4762–4774. [CrossRef]

20. Prihodko, L.; Goward, S.N. Estimation of air temperature from remotely sensed surface observations. *Remote Sens. Environ.* **1997**, *60*, 335–346. [CrossRef]

21. Stisen, S.; Sandholt, I.; Nørgaard, A.; Fensholt, R.; Eklundh, L. Estimation of diurnal air temperature using MSG SEVIRI data in West Africa. *Remote Sens. Environ.* **2007**, *110*, 262–274. [CrossRef]

22. Vancutsem, C.; Ceccato, P.; Dinku, T.; Connor, S.J. Evaluation of MODIS land surface temperature data to estimate air temperature in different ecosystems over Africa. *Remote Sens. Environ.* **2010**, *114*, 449–465. [CrossRef]

23. Wan, Z.; Hook, S.; Hulley, G. MOD11A1 MODIS/Terra Land Surface Temperature/Emissivity Daily L3 Global 1km SIN Grid V006 [Data set]. *NASA EOSDIS LP DAAC* **2015**. [CrossRef]

24. Wan, Z.; Hook, S.; Hulley, G. MYD11A1 MODIS/Aqua Land Surface Temperature/Emissivity Daily L3 Global 1km SIN Grid V006 [Data set]. *NASA EOSDIS LP DAAC* **2015**. [CrossRef]

25. Shah, D.B.; Pandya, M.R.; Trivedi, H.J.; Jani, A.R. Estimating minimum and maximum air temperature using MODIS data over Indo-Gangetic Plain. *J. Earth Syst. Sci.* **2013**, *122*, 1593–1605. [CrossRef]

26. Zhu, W.; Lŭ, A.; Jia, S. Estimation of daily maximum and minimum air temperature using MODIS land surface temperature products. *Remote Sens. Environ.* **2013**, *130*, 62–73. [CrossRef]

27. Williamson, S.; Hik, D.; Gamon, J.; Kavanaugh, J.; Flowers, G. Estimating temperature fields from MODIS land surface temperature and air temperature observations in a sub-arctic alpine environment. *Remote Sens.* **2014**, *6*, 946–963. [CrossRef]

28. Pepin, N.; Deng, H.; Zhang, H.; Zhang, F.; Kang, S.; Yao, T. An examination of temperature trends at high elevations across the Tibetan Plateau: The use of MODIS LST to understand patterns of elevation-dependent warming. *J. Geophys. Res. Atmos.* **2019**, *124*, 5738–5756. [CrossRef]

29. Singh, S.; Kumar, R.; Bhardwaj, A.; Sam, L.; Shekhar, M.; Singh, A.; Kumar, R.; Gupta, A. The Indian Himalayan Region: A review of signatures of changing climate and vulnerability. *WIREs Clim. Chang.* **2016**, *7*, 393–410. [CrossRef]

30. Immerzeel, W.W.; Van Beek, L.P.H.; Bierkens, M.F.P. Climate Change Will Affect the Asian Water Towers. *Science* **2010**, *328*, 1382–1385. [CrossRef]

31. Sam, L.; Bhardwaj, A.; Kumar, R.; Buchroithner, M.F.; Martín-Torres, F.J. Heterogeneity in topographic control on velocities of Western Himalayan glaciers. *Sci. Rep.* **2018**, *8*, 12843. [CrossRef] [PubMed]

32. Sam, L.; Bhardwaj, A.; Sinha, V.S.P.; Joshi, P.K.; Kumar, R. Use of Geospatial Tools to Prioritize Zones of Hydro-Energy Potential in Glaciated Himalayan Terrain. *J. Indian Soc. Remote Sens.* **2016**, *44*, 409–420. [CrossRef]

33. Shekhar, M.; Bhardwaj, A.; Singh, S.; Ranhotra, P.S.; Bhattacharyya, A.; Pal, A.K.; Roy, I.; Martín-Torres, F.J.; María-Paz, Z. Himalayan glaciers experienced significant mass loss during later phases of little ice age. *Sci. Rep.* **2017**, *7*, 10305. [CrossRef] [PubMed]

34. Bookhagen, B.; Burbank, D.W. Toward a complete Himalayan hydrological budget: Spatiotemporal distribution of snowmelt and rainfall and their impact on river discharge. *J. Geophys. Res.* **2010**, *115*. [CrossRef]

35. National Centre for Environmental Information (NCEI). Available online: https://www.ncei.noaa.gov/ (accessed on 5 November 2019).

36. Villarini, G.; Khouakhi, A.; Cunningham, E. On the impacts of computing daily temperatures as the average of the daily minimum and maximum temperatures. *Atmos. Res.* **2017**, *198*, 145–150. [CrossRef]

37. Ma, Y.; Guttorp, P. Estimating daily mean temperature from synoptic climate observations. *Int. J. Climatol.* **2013**, *33*, 1264–1269. [CrossRef]

38. NASA Earthdata Portal. Available online: https://earthdata.nasa.gov/ (accessed on 5 November 2019).

39. Wan, Z. New refinements and validation of the MODIS land-surface temperature/emissivity products. *Remote Sens. Environ.* **2008**, *112*, 59–74. [CrossRef]

40. Shah, H.L.; Zhou, T.; Huang, M.; Mishra, V. Strong influence of irrigation on water budget and land surface temperature in Indian sub-continental river basins. *J. Geophys. Res. Atmos.* **2019**, *124*, 1449–1462. [CrossRef]

41. Goddard Earth Sciences Data and Information Services Center. *TRMM (TMPA) Precipitation L3 1 Day 0.25 Degree × 0.25 Degree V7*; Savtchenko, A., Ed.; GES DISC: Greenbelt, MD, USA, 2016. [CrossRef]

42. Williamson, S.N.; Hik, D.S.; Gamon, J.A.; Jarosch, A.H.; Anslow, F.S.; Clarke, G.K.; Rupp, T.S. Spring and summer monthly MODIS LST is inherently biased compared to air temperature in snow covered sub-Arctic mountains. *Remote Sens. Environ.* **2017**, *189*, 14–24. [CrossRef]

43. Immerzeel, W.W.; Petersen, L.; Ragettli, S.; Pellicciotti, F. The importance of observed gradients of air temperature and precipitation for modeling runoff from a glacierized watershed in the Nepalese Himalayas. *Water Resour. Res.* **2014**, *50*, 2212–2226. [CrossRef]

44. Singh, S.; Kumar, R.; Bhardwaj, A.; Kumar, R.; Singh, A. Changing climate and glacio-hydrology: A case study of Shaune Garang basin, Himachal Pradesh. *Int. J. Hydrol. Sci. Technol.* **2018**, *8*, 258–272. [CrossRef]

45. Singh, P.; Haritashya, U.K.; Kumar, N. Modelling and estimation of different components of streamflow for Gangotri Glacier basin, Himalayas. *Hydrol. Sci. J.* **2008**, *53*, 309–322. [CrossRef]

46. Wulf, H.; Bookhagen, B.; Scherler, D. Differentiating between rain, snow, and glacier contributions to river discharge in the western Himalaya using remote-sensing data and distributed hydrological modeling. *Adv. Water Resour.* **2016**, *88*, 152–169. [CrossRef]

47. Kraaijenbrink, P.D.A.; Bierkens, M.F.P.; Lutz, A.F.; Immerzeel, W.W. Impact of a global temperature rise of 1.5 degrees Celsius on Asia's glaciers. *Nature* **2017**, *549*, 257–260. [CrossRef]

48. Shekhar, M.S.; Chand, H.; Kumar, S.; Srinivasan, K.; Ganju, A. Climate-change studies in the western Himalaya. *Ann. Glaciol.* **2010**, *51*, 105–112. [CrossRef]

49. Liang, E.; Dawadi, B.; Pederson, N.; Eckstein, D. Is the growth of birch at the upper timberline in the Himalayas limited by moisture or by temperature? *Ecology* **2014**, *95*, 2453–2465. [CrossRef]

50. Xu, J.; Grumbine, R.E.; Shrestha, A.; Eriksson, M.; Yang, X.; Wang, Y.; Wilkes, A. The Melting Himalaya: Cascading Effects of Climate Change on Water, Biodiversity, and Livelihoods. *Conserv. Biol.* **2009**, *23*, 520–530. [CrossRef]

51. Archer, D.R.; Forsythe, N.; Fowler, H.J.; Shah, S.M. Sustainability of water resources management in the Indus Basin under changing climatic and socio economic conditions. *Hydrol. Earth Syst. Sci.* **2010**, *14*, 1669–1680. [CrossRef]

52. Malla, G. Climate Change and Its Impact on Nepalese Agriculture. *J. Agric. Environ.* **2009**, *9*, 62–71. [CrossRef]

53. Kimball, J.S.; Running, S.W.; Nemani, R. An improved method for estimating surface humidity from daily minimum temperature. *Agric. For. Meteorol.* **1997**, *85*, 87–98. [CrossRef]

54. Good, E.J. An in situ-based analysis of the relationship between land surface "skin" and screen-level air temperatures. *J. Geophys. Res. Atmos.* **2016**, *121*, 8801–8819. [CrossRef]

55. Good, E.J.; Ghent, D.J.; Bulgin, C.E.; Remedios, J.J. A spatiotemporal analysis of the relationship between near-surface air temperature and satellite land surface temperatures using 17 years of data from the ATSR series. *J. Geophys. Res. Atmos.* **2017**, *122*, 9185–9210. [CrossRef]

56. Kulkarni, A.V.; Rathore, B.P.; Singh, S.K. Distribution of seasonal snow cover in central and western Himalaya. *Ann. Glaciol.* **2010**, *51*, 123–128. [CrossRef]

57. Bhardwaj, A.; Singh, S.; Sam, L.; Bhardwaj, A.; Martin-Torres, F.J.; Singh, A.; Kumar, R. MODIS-based estimates of strong snow surface temperature anomaly related to high altitude earthquakes of 2015. *Remote Sens. Environ.* **2017**, *188*, 1–8. [CrossRef]

58. Niclos, R.; Valiente, J.A.; Barberà, M.J.; Caselles, V. Land surface air temperature retrieval from EOS-MODIS images. *IEEE Geosci. Remote Sens. Lett.* **2013**, *11*, 1380–1384. [CrossRef]